Optical properties and ferromagnetic order in K2 CuF4

W. Kleemann, Y. Farge

Classification
Physics Abstracts
8.824 — 8.514 — 8.818

OPTICAL PROPERTIES AND FERROMAGNETIC ORDER IN K_2CuF_4

W. KLEEMANN (*) and Y. FARGE

Laboratoire de Physique des Solides (**), Université Paris-Sud, 91405 Orsay, France

(*Reçu le 11 juin 1975, accepté le 18 août 1975*)

Résumé. — Dans cet article, une analyse du champ cristallin agissant sur le multiplet $3d^9$ de l'ion Cu^{++} dans K_2CuF_4 est présentée, à partir des mesures d'absorption optique, de dichroïsme linéaire et d'anisotropie du tenseur **g**. Pour interpréter les résultats, il est nécessaire de prendre en compte une symétrie locale D'_{4h}, qui est due à des octaèdres de F^- allongés, ayant leurs axes tétragonaux dans les plans c, configuration proposée théoriquement et confirmée par des études de diffraction de rayons X. Une distorsion supplémentaire orthorhombique est nécessaire pour expliquer les propriétés dichroïques.

Le dichroïsme circulaire magnétique, la rotation Faraday et la dépendance de la biréfringence avec un champ magnétique sont utilisés pour mesurer des courbes d'aimantation dans le plan et perpendiculairement au plan en dessous de $T_c = 6{,}25$ K. La dispersion rotatoire Faraday dans le visible et des effets de domaines sont discutés.

Abstract. — A crystal field analysis of the $3d^9$ multiplet of Cu^{++} in K_2CuF_4 is presented, taking into account optical absorption spectra, linear dichroism, and the anisotropy of the **g** tensor. The calculations are based on local D'_{4h} symmetry arising from elongated ligand octahedra with their long axes in the c planes, as it has been proposed theoretically and confirmed by X-ray studies. An additional orthorhombic distortion must be assumed to explain the dichroic properties.

Magnetic circular dichroism, Faraday rotation, and magnetic field dependence of the linear birefringence have been used to measure in- and out-of-plane magnetization curves below $T_c = 6.25$ K. The Faraday rotary dispersion in the visible region and domain effects are discussed.

1. **Introduction.** — In the last few years growing interest has been focused on materials exhibiting magnetic properties, which are dominantly one- or two-dimensional [1]. Among these, the ionic layer compounds crystallizing in the K_2NiF_4 structure (tetragonal face centered, space group D_{4h}^{17}) are particularly well understood. The best known examples are K_2MnF_4, K_2NiF_4 and K_2CuF_4. In these crystals nearly isotropic two-dimensional (2 D) spin-order is established in the c-planes (perpendicular to the tetragonal *c*-axis). Such systems are expected to exhibit no long-range order at finite temperatures [2], but a transition into a phase with divergent susceptibility should occur at a finite temperature $T_c^{(2)}$ [3].

Actually in all cases a transition into 3 D long-range order is observed at a critical temperature T_c in the vicinity of the Stanley-Kaplan temperature $T_c^{(2)}$. This is due to deviations from the pure Heisenberg exchange interaction and (or) to a small, but finite interlayer exchange.

Among the ferromagnets having the K_2NiF_4 structure only two 2 D systems are known : K_2CuF_4 [4, 5] and Rb_2CuF_4 [6]. Other crystals, such as K_2CrCl_4 [7], Rb_2CrCl_4 [8] and Cs_2CrCl_4 [9], exhibit 3 D ferromagnetism. In K_2CuF_4, the best studied of all these systems, the ratio between inter- and intraplane exchange is only $J'/J \approx 3 \times 10^{-3}$, where $J/k_B \sim 10$ K. About 1 % *xy*-like anisotropy is found in the intraplane exchange. The transition into 3 D order takes place at $T_c = 6.25$ K, where a small peak in the specific heat is detected [5]. The spontaneous magnetization lies parallel to one of the *a*-axes. Thus four different types of magnetic domains can be expected.

Above T_c the magnetic properties of K_2CuF_4 are determined by 2 D short-range order. This manifests quite clearly in the departure of the susceptibility from the Curie-Weiss behaviour at temperatures as high as 10 T_c [5], and in the occurrence of a flat peak in the magnetic specific heat c_m at about 1.5 T_c [5].

In this paper we wish to report the results of optical measurements on K_2CuF_4. It is well-known that the magnetic properties of a crystal are reflected by many of its optical properties. In a preceding letter [10] we have already shown that the magnetic short-range order determines the linear magnetic bire-

(*) Present address : I. Physikalisches Institut der Universität, D 34 Göttingen, Bunsenstr. 9, FRG.

(**) Laboratoire associé au C.N.R.S.

fringence (LMB) and the temperature shift of a zero-phonon line in the near infrared. Both properties are found to be proportional to the internal magnetic energy U_m, which is proportional to the short-range order parameter $\langle \mathbf{S}.\mathbf{S}_a \rangle$ in a good first approximation.

The mechanism involved in the LMB is the magnetostriction being proportional to $\langle \mathbf{S}.\mathbf{S}_a \rangle$ according to the compressible lattice model proposed by Jahn and Dachs [11]. Convincing evidence for the relation LMB $\propto \langle \mathbf{S}.\mathbf{S}_a \rangle$ has also been found in K_2MnF_4 [12] and K_2NiF_4 [13]. The line shift, on the other hand, is proportional to the exchange stabilization of the Cu^{2+} ground state, which again is determined by the local spin order.

In the present study we have investigated magneto-optical effects, which are related to the magnetization $\langle S_z \rangle$ in the ordered state below T_c. It will be shown that the magnetic circular dichroism (MCD) and the Faraday rotation are both proportional to the macroscopic magnetization induced by an external magnetic field. It is also possible to measure the spontaneous magnetization as a function of T on a single domain. The influence of an external field on the linear birefringence and its relation to magnetization is studied. The rotary dispersion in the transparent region of the crystal will be discussed in terms of a simple dispersion law.

The absorption bands in the near infrared [10] correspond to the d-d transitions of the Cu^{2+} ion. They will be discussed using the results of absorption spectra and linear dichroism. A consistent crystal field analysis proves to be possible only with a new structure model of K_2CuF_4, which has been proposed by Khomskii and Kugel [14]. These authors predicted that the lattice of K_2CuF_4 undergoes a cooperative ordering due to the Jahn-Teller effect and to the superexchange mechanism at low temperatures. Taking into account both effects simultaneously, the Cu^{2+} ions are expected to be surrounded by elongated ligand (F^-) octahedra, the long axes of which lying alternatively parallel to the a and a' axis of the crystal (a and a' span the c-plane). In order to explain the dichroic properties of the absorption spectrum a supplementary orthorhombic distortion of the local octahedra must be assumed.

2. **Experimental procedure.** — Single crystals of K_2CuF_4 (size $6 \times 6 \times 1$ mm^3) of good optical quality produced by Cristaltec, Grenoble, France, have been used in our experiments. Axial (α) absorption, MCD, and Faraday rotation were measured on a sample cleaved parallel to the c-plane (sample I). π and σ spectra were obtained on a sample, whose faces were parallel to the c-axis (sample II). Before each measurement the samples were carefully polished in order to remove thin surface layers due to hygroscopic reactions.

The cryostat used in the experiments allowed measurements between 1.6 and 4.2 K by use of pumped helium. Between 4.2 and 300 K, temperature stabilization of 0.1 K was achieved by heating the sample holder against cold helium gas. The sample was located in the bore of a small supraconducting solenoid providing magnetic fields up to 30 kOe parallel to the direction of the monitor light beam.

Optical absorption between 0.25 and 2 μ wavelength was measured with a Cary 14 spectrophotometer. In the near infrared ($\lambda \sim 1.1$ μ) its PbS detector allowed a spectral resolution $s \sim 5$-10 cm^{-1}. Between 2.5 and 16 μ a Perkin Elmer No. 237 spectrometer was used to locate the lowest excited state of the Cu^{2+} ions. Higher resolution in the near infrared was obtained with a Jarrell-Ash 1 m Czerny-Turner scanning monochromator combined with a 500 W Xenon high pressure lamp and a cooled photomultiplier (150 CVP). Since the sharp lines to be investigated [10] lie in a spectral range of high underground absorption, the resolution was noise-limited to $s \sim 5$ cm^{-1}. Linear dichroism between 0.7 and 2 μ was measured by inserting HR polarizers into the monitor and the reference beams of the Cary spectrophotometer. In order to measure $\pi(\sigma)$ absorption, the electric light vector was directed parallel (perpendicular) to the c-axis of sample II.

MCD measurements were performed with what is now classical equipment and has been described elsewhere [15]. This apparatus gives directly the circular polarization rate versus wavelength. This rate is proportional to $\alpha_+ - \alpha_-$ provided that $|(\alpha_+ - \alpha_-)\, d| \ll 1$ (α_+, α_- = absorption coefficients for right and left circularly polarized light, respectively; d = crystal thickness).

The Faraday rotation was measured by placing the sample between crossed Glan polarizers. The magnetic field induced rotation of the plane of polarization was compensated by turning the analyzer by an appropriate angle θ. The intensity minimum was detected by common lock-in technique. The accuracy thus obtained ($\Delta\theta = \pm 0.5°$) proved to be sufficient in the present investigation.

Linear birefringence measurements with an absolute error of Δn of about 2×10^{-6} are carried out with an apparatus previously described [13]. We have measured magnetic field effects on the linear birefringence owing to domain orientation.

3. **Experimental results.** — 3.1 Optical Absorption and Linear Dichroism. — Axial (α) absorption spectra recorded at different temperatures between 295 and 1.7 K in the wavelength range from 0.25 to 16 μ are shown in figure 1. Very strong absorption ($\alpha > 60$ cm^{-1}) is found in the UV below 0.25 μ and in the IR above 13 μ. These edges are interpreted to be due to dipole-allowed charge transfer transitions of the Cu^{2+} ions (UV), and to the fundamental lattice absorption (IR), respectively.

In the near IR a broad, structured band (halfwidth

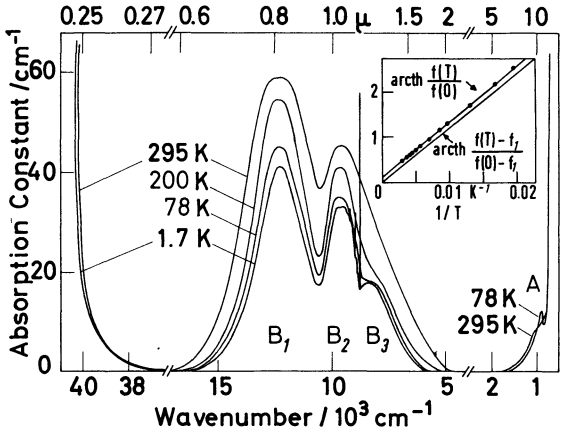

FIG. 1. — Axial absorption spectra of K_2CuF_4, obtained at temperatures between 1.7 and 295 K. A, B_1, B_2 and B_3 denote the bands referring to the excited states of the Cu^{2+} ion. Insert : Temperature dependence of the oscillator strength of B_1, B_2, and B_3.

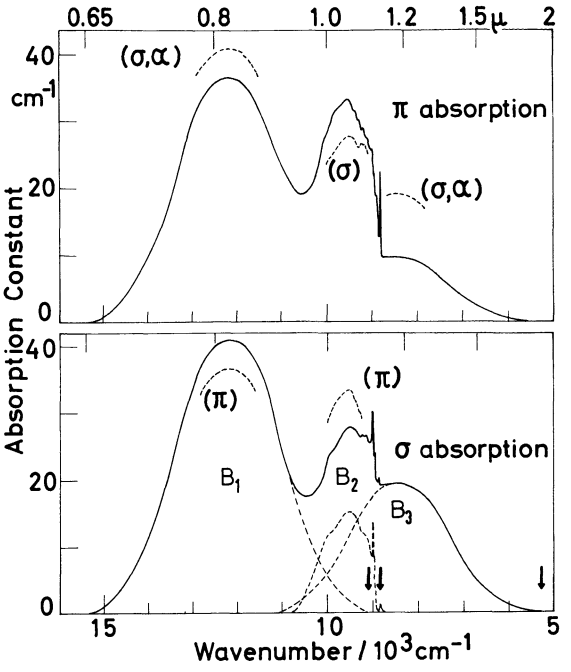

FIG. 2. — π and σ absorption of the bands B_1, B_2 and B_3 at 1.7 K. The σ spectrum has been decomposed into three single bands (dashed lines). The positions of the respective zero-phonon lines are indicated by arrows.

about 6 000 cm^{-1}) is dominating. It extends into the visible region until about 0.6 μ. This gives rise to the pale-blue color of K_2CuF_4 at room temperature. This color fades away at low temperatures, since the absorption edge moves to the IR. At the same time the overall absorption decreases and the band becomes resolved into three peaks B_1, B_2 and B_3 at 12 200, 9 400 and 8 400 cm^{-1}, respectively. A fourth small peak (A) appears in the high energy slope of the lattice absorption at 970 cm^{-1}.

The four IR bands correspond to transitions within the $3d^9$ multiplet of the Cu^{2+} ion. These transitions are parity-forbidden and become slightly allowed by vibrational interaction. This explains the increase of the overall oscillator strength f with increasing temperature. We find $f(300\ K)/f(0) = 2.16$ and $f(0) = 1.9 \times 10^{-5}$, assuming a refractive index of $n = 1.5$ to account for the internal field correction. A plot of arcoth $f(T)/f(0)$ versus $1/T$ should yield a straight line passing through the origin, provided that the transitions are only due to the phonon assisted electric dipole mechanism. As can be seen from the insert in figure 1, the straight line interpolating our arcoth $f(T)/f(0)$ values does not end in the origin. It will be shown in 4.2.1 that this behaviour is due to a non-negligible magnetic dipole contribution to the oscillator strength.

The near IR bands exhibit a considerable linear dichroism. This is seen in figure 2 which shows the low temperature π, σ and α spectra. In π absorption, B_3 decreases by 50 % as compared with σ and α. A similar decrease, but only by 10 %, is found in B_1. On the other hand, B_2 is strongly π polarized. In σ and α absorption it decreases by 45 % and 25 %, respectively, in comparison with its π absorption strength. These values have been obtained after subtraction of the overlapping bands at both sides of B_2. The dichroism is independent from temperature up to about 60 K, where the increasing overlap of the three bands (see Fig. 1) tends to diminish dichroic effects.

Below about 50 K a rich fine structure appears in B_2. This is shown in detail in figure 3 for α, σ and π absorption. At least ten well resolved peaks are found

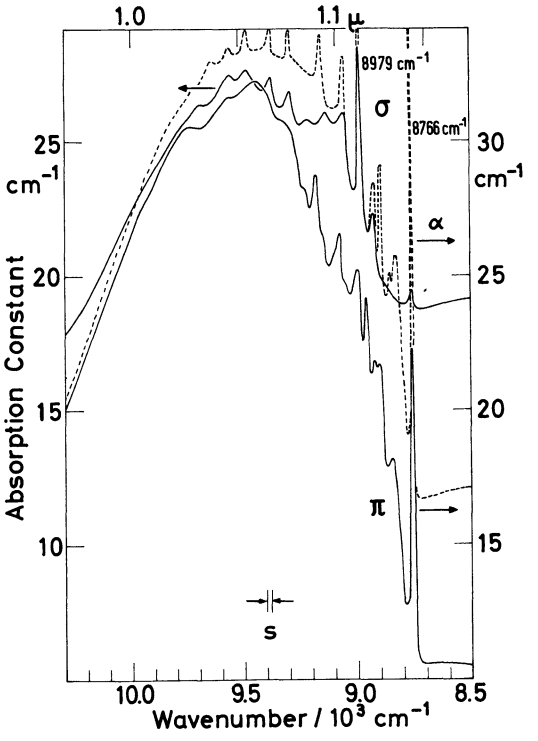

FIG. 3. — Fine structure of the B_2 band at 1.7 K in α, π and σ polarization (α, π : righthand, σ : lefthand ordinate scale). Spectral resolutions : $s(\alpha) \sim 5\ cm^{-1}$, $s(\sigma, \pi) \sim 10\ cm^{-1}$.

in either polarization. As has been reported earlier [10], two lines at 8 766 and 8 979 cm^{-1} ([1]) are particularly intense and narrow (halfwidths at 1.7 K : $h \sim 5\ cm^{-1}$). As can be seen in figure 3, they are strongly dichroic. The 8 766 cm^{-1} line appears in π and α, but vanishes nearly completely in the σ spectrum. The remaining absorption is presumably due to a slight misorientation of the sample. On the other hand, the 8 979 cm^{-1} line is strongly σ and α polarized. It is the most prominent line in the σ spectrum. The corresponding line in the π spectrum is rather weak. Apart from the sharp lines, dichroism is also found in the other peaks (see Fig. 3).

It has to be noted that only the α spectrum, as presented in figure 3, is completely resolved ($s \sim 5\ cm^{-1}$). The π and σ spectra could only be obtained with $s \sim 10\ cm^{-1}$ because of the absorbing polarizers inserted into the spectrometer beams.

It will be shown in 4.2 that the positions of the absorption bands can be predicted by crystal field theory, and that B_2 contains dipolar electric and magnetic contributions.

3.2 MAGNETIC CIRCULAR DICHROISM. — 3.2.1 *Axial applied magnetic field.* — Magnetic fields applied parallel to the c-axis of sample I give rise to MCD within all near IR absorption bands. Special attention is paid to the behaviour of the narrow lines. Figure 4 shows the MCD of the 8 766 cm^{-1} line at 4.2 K, subtracted from the flat signal of the underlying broad band and normalized to the line peak absorption. Within the experimental error the MCD line shape coincides with that of the absorption line. Unfortunately the MCD signals are strongly perturbed by detector shot-noise which becomes significant at low light levels which were needed in order to realize a high spectral resolution.

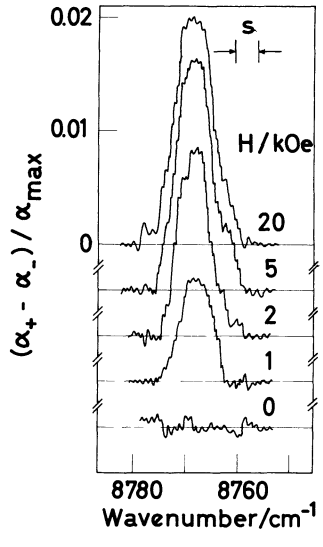

FIG. 4. — Magnetic circular dichroism of the 8 766 cm^{-1} line at 4.2 K in axial magnetic fields up to 20 kOe.

([1]) The energy values reported in reference [10] had to be corrected after a new spectrometer calibration.

Preliminary measurements of the broad band MCD have also been carried out. Correlations are found between MCD peaks and the vibronic structure of B_2. Details of the rather complex MCD spectrum will be presented in a subsequent paper.

In this paper we restrict our discussion to the saturation behaviour of the MCD, which is found in the whole absorption range. Figure 4 shows that saturation is achieved in fields exceeding about 5 kOe. This behaviour suggests that the circular dichroism arises rather from the molecular field due to ferromagnetic order than from the external field H. In a simple picture we may expect that H rotates the spontaneous magnetization M_s from the easy c-plane [5] into c-direction, thus overcoming the out-of-plane anisotropy field. The component of M parallel to c, being equal to the macroscopic magnetization $M(H)$, gives rise to a longitudinal Zeeman effect, which is detected by the MCD.

This property allows a measurement of qualitative magnetization curves with high precision. Figure 5 shows one of these curves obtained at $T = 4.2$ K and $\lambda = 660$ nm (full line). Within the limits of experimental error ($\pm$ 0.002) the curve proves to be exactly reproducible without any hysteresis. This seems to characterize the high quality of our sample. A saturation value of $|(\alpha_+ - \alpha_-)/\alpha| = 0.22$ is achieved for $|H| \simeq 8$ kOe. The dashed line in figure 5 represents $M(H_i)$, where $H_i = H - NM$ is the internal field corrected for the demagnetization field. Note that the abscissa now reads H_i. The conversion is performed with $N = 0.79 \times 4\pi$ (demagnetization factor of sample I, assuming an ellipsoidal shape with the axis ratio $c/a = 6$), and with Yamada's saturation value [5] $M_s = 76$ emu/cm^3. It is seen that $M = 0.7\ M_s$ is obtained with $H_i \sim 1$ kOe. As will be shown in 4.3.1, the magnetization curve allows an estimation of the out-of-plane anisotropy field.

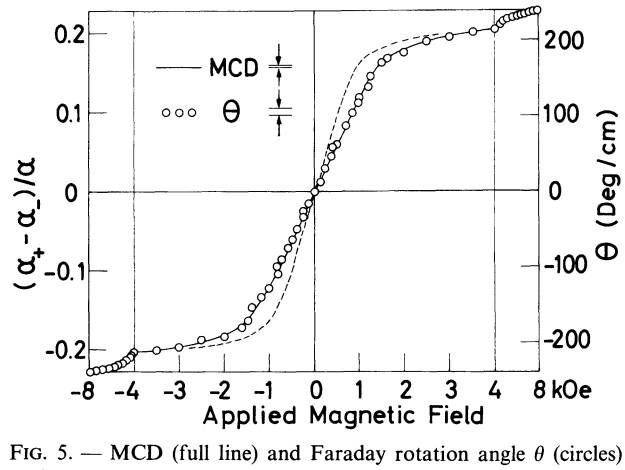

FIG. 5. — MCD (full line) and Faraday rotation angle θ (circles) as functions of axial magnetic field strength, obtained at 660 nm and 4.2 K. The dashed line represents the magnetization in arbitrary units as a function of the internal magnetic field (abscissa scale).

3.2.2 *Non-axial applied magnetic field; domain effects.* — MCD measurements with non-axial magnetic fields are more difficult to interpret. Non-vanishing signals at zero applied field indicate that linear dichroism (see 3.1) and natural birefringence [10] give rise to spurious effects. However, these effects prove to be small as compared with the MCD in favorable spectral regions. At 660 nm, for example, the linear dichroism is nearly negligible (see Fig. 2). The CD at $H = 0$ obtained on sample II (**H** // **a**) is therefore only due to the birefringence. Subtracting this signal from the MCD versus H curve, we find a magnetization curve saturating at $H \sim 1.0$ kOe, which corresponds to $H_i \sim 250$ Oe. This result, though less reliable than the results for **H** // **c**, demonstrates the nearly vanishing in-plane anisotropy [5]. A similar result is obtained from linear birefringence data (see 3.4 and 4.5).

Single domain effects were also observed on sample I, when it was orientated with its c-axis under an angle of 45° with respect to the monitor light beam. In this geometry CD signals are found at $H = 0$. They vary in strength and even in sign for different positions and diameters of the incident light beam. Obviously, single domains are probed, since they are magnetized parallel to the c-plane and thus exhibit a magnetization component in the light direction. This effect should provide a means to determine the domain structure as is planned in future experiments.

Preliminary measurements between 1.6 and 4.2 K have shown that the zero field CD signal decreases like the spontaneous magnetization M_s [16, 17]. Further experiments are planned to measure $M_s(T)$ up to $T = T_c$ by means of this new optical technique.

3.3 Faraday Rotation. — Circular dichroism is always accompanied by circular birefringence. If the CD is magnetic field induced, the crystal exhibits a Faraday rotation. This may be used like MCD to measure relative magnetization curves $M(H)$ in an ordered ferromagnet. Figure 5 shows the result obtained at 4.2 K with 660 nm light for sample I in axial magnetic fields (circles). The curve thus obtained coincides exactly with the MCD curve, using a matched scale representation. Saturation rotation angles $\theta = \pm 238°$/cm are obtained with $H_{appl} = \pm 8$ kOe. The scatter of the experimental θ values, being four times greater than that of the MCD values, might easily be reduced by more sophisticated experimental techniques (see e.g. ref. [18]). The dashed curve in figure 5, M versus H_i, applies, too, to the rotation measurement, since both, MCD and θ, were obtained on the same sample.

The rotary dispersion $\theta(\lambda)$ has been measured between 380 and 700 nm at 4.2 K with a saturating axial field ($H = 10$ kOe). We find a monotonous increase of θ between 700 nm ($\theta = 160°$/cm) and 380 nm ($\theta = 1\,080°$/cm). In the transparent region below 630 nm (see Fig. 1) the data are well described by the function

$$\theta = B/(\lambda^2 - \lambda_0^2) . \qquad (1)$$

The best fit parameters $\lambda_0 = 235$ nm and

$$B = 1.03 \times 10^8 \text{ (deg/cm) nm}^2$$

are obtained from a plot of θ^{-1} versus λ^2 as shown in figure 6.

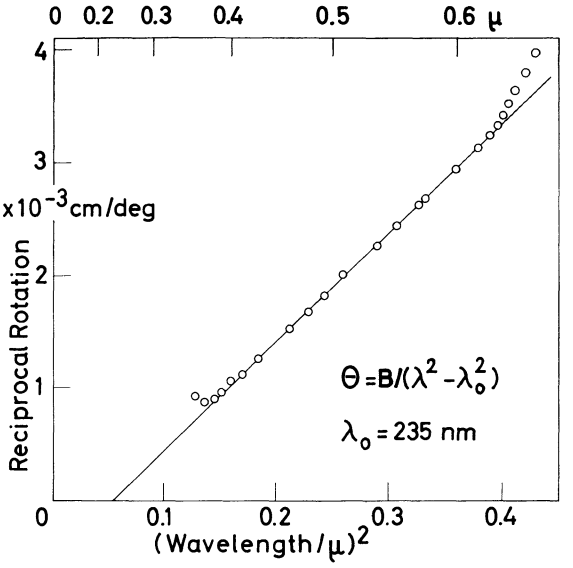

FIG. 6. — Reciprocal Faraday rotation angle θ^{-1} as function of λ^2, obtained at 4.2 K and $H = 10$ kOe. The straight line refers to the dispersion law $\theta = B/(\lambda^2 - \lambda_0^2)$.

Eq. (1) is the simplified theoretical expression for the Faraday rotation assuming only one strong optical transition at the resonance wavelength λ_0 [19]. In our case λ_0 represents a mean wavelength corresponding to the very strong charge transfer transitions of K_2CuF_4, which give rise to the absorption edge at about 240 nm (Fig. 1).

The constant B is mainly determined by the magnetization $\langle S_z \rangle$ and the oscillator strength f_{UV} of the transition at λ_0 [19] :

$$B \propto (n_0^2 + 2)\, \lambda_0^2\, f_{UV} \langle S_z \rangle / n_0 , \qquad (2)$$

where n_0 is the mean refraction index of the crystal being virtually constant in the transparent region. In the vicinity of the UV absorption edge, however, n_0, and consequently B will depend on λ as well. This is probably one reason for the non-linear behaviour of θ^{-1} versus λ^2 below 400 nm (see Fig. 6).

It is evident from relation (2) that weak transitions such as those in the near IR ($f \sim 10^{-3}\, f_{UV}$) exert practically no influence on θ in the transparent region. This changes, however, in the absorption region above 630 nm, where resonance terms of the form $(\lambda^2 - \lambda_i^2)^{-1}$ become important in θ (λ_i = resonance wavelengths of the IR transitions). This explains the breakdown of eq. (2) above 630 nm as is illustrated by some experimental points in figure 6.

3.4 MAGNETIC FIELD EFFECTS ON LINEAR BIREFRINGENCE. — Owing to its tegragonal lattice structure, K_2CuF_4 is unaxially birefringent. Below 100 K the temperature dependent contribution to the linear birefringence is mainly due to 2 D spin order [10]. Below T_c the crystal will become biaxially birefringent because of an additional magnetostriction within the c-plane, since the magnetization lies parallel to one of the a-axes [5]. The lattice structure will become orthorhombic with the crystal axes c, a_1 and a_2 where $\mathbf{M} /\!/ \mathbf{a}_2$, but $\mathbf{M} \perp \mathbf{c}$, $\mathbf{a}_1$.

Evidence of the orthorhombic distortion below T_c is obtained from the magnetic field dependence of the linear birefringence in the ac-plane (sample II) for **H** parallel to the direction of light propagation. The experimental data $|\Delta n(H) - \Delta n(0)|$ at 1.8 K are plotted versus H in figure 7, where $\Delta n = n_e - n_0$ is the linear birefringence as measured with a HeNe laser beam ($\lambda = 632.8$ nm) having a diameter of about 1 mm. At $H \sim 1$ kOe a total change of the birefringence of 2.3×10^{-5} is observed, which is about 20 % of the total LMB [10]. The change of Δn proves to be independent from the sign of H.

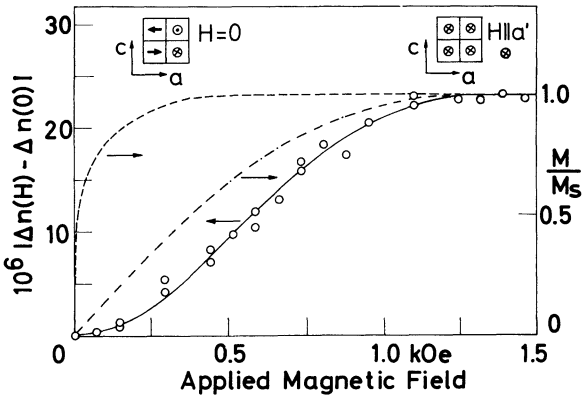

FIG. 7. — Linear birefringence $|\Delta n(H) - \Delta n(0)|$, measured at 1.8 K and 632.8 nm in the ac-plane with **H** parallel to **a'** (circles, lefthand ordinate scale). Relative magnetization M/M_s (righthand ordinate scale), calculated from the linear birefringence (interpolated full line), is shown as function of the applied field (dot-dashed curve) and the internal field (dashed curve), respectively.

This effect can be explained as follows. In zero applied field four different types of domains are probed by the laser beam (lefthand insert of figure 7). Thus we measure $\Delta n(0) = n_c - n_{a1,a2}$, where $n_{a1,a2}$ is the mean index of refraction for light polarized parallel to $\mathbf{a}_1$ and $\mathbf{a}_2$, respectively. An external field **H** turns the domains into its direction (righthand insert of figure 7). In the limit of saturating field strength only domains with their $\mathbf{a}_1$ axis parallel to the sample face are probed. Thus we obtain $\Delta n(H_{sat}) = n_c - n_{a1}$ (principal birefringence). A similar effect, measured in a transverse magnetic field, has been observed on the canted antiferromagnet NiF_2 [11], where, however, the in-plane birefringence $|n_{a1} - n_{a2}|$ is only 1 % of the total LMB.

It will be shown in 4.3.2 that the field dependence of Δn is related to the magnetization, thus allowing a determination of the in-plane magnetization curve.

4. **Discussion.** — 4.1 CRYSTALLOGRAPHIC STRUCTURE OF K_2CuF_4. — It has been pointed out by Khomskii and Kugel [14] that the K_2NiF_4 lattice structure as determined by Knox [20] cannot explain the ferromagnetic interaction in K_2CuF_4. They proposed a low temperature phase as a result of a cooperative Jahn-Teller distortion, where the Cu^{2+} ions are expected to be surrounded by elongated ligand octahedra with their long axes being alternatively parallel to the x and y axis of the crystal (x and y span the c-plane, see figure 8 : coordinate system I). In this model the ground state wavefunctions transform alternatively like $z^2 - x^2$ and $z^2 - y^2$, respectively. The superexchange interaction between two neighbouring ions along the x or y axis vanishes, because their wave functions are orthogonal, whereas the exchange interaction along the diagonal of the square is positive. Such a cooperative Jahn-Teller effect has also been observed in $(CH_3NH_3)_2CuCl_4$, where the Cu^{2+} ions, too, form a planar square lattice [21].

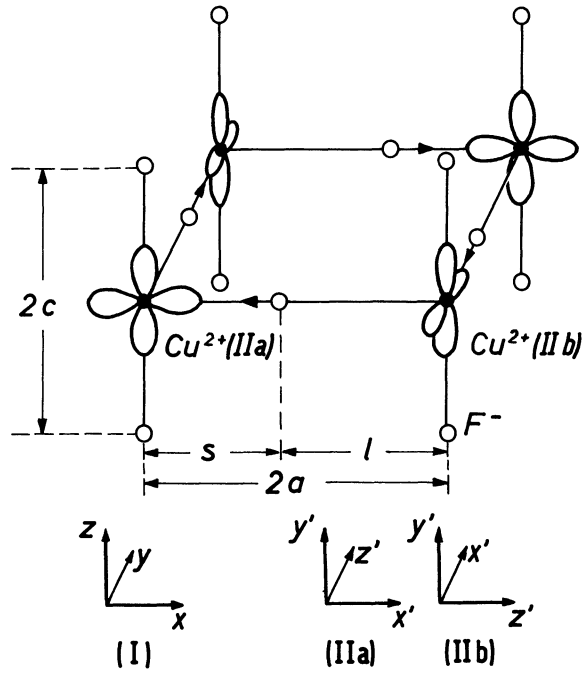

FIG. 8. — Crystal structure of the basal plane in K_2CuF_4 (after ref. [14]). The ordering of the hole orbitals is shown. The corresponding displacements of F^- ions are marked by arrows. The coordinate systems refer to the crystal axes (I), and to the local octahedron axes (II*a* and II*b*), respectively.

In order to observe the above described Jahn-Teller distortion, an X-ray diffraction experiment has been performed with a monochromatic X-ray beam propagating along the c-axis ([2]) (Fig. 9). The

([2]) We are pleased to thank F. Denoyer, who has done this experiment.

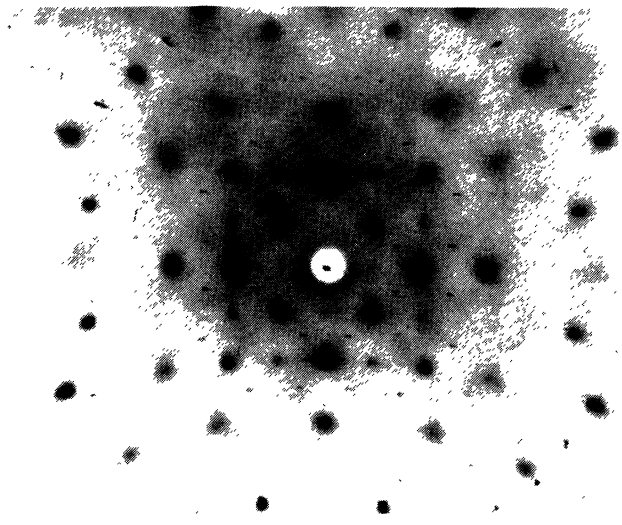

FIG. 9. — Monochromatic Laüe diffraction pattern of K_2CuF_4, obtained at 300 K with Co K_α radiation, propagating parallel to the fourfold c axis.

Bragg reflections of the undistorted structure are seen on dotted line hyperbolae. Between these reflections, due to the ordinary K_2NiF_4 structure, a series of dots can be observed. They correspond to the expected superstructure with a doubled unit cell along x and y. Measurements at 300 and 77 K have shown essentially the same diffraction pattern. This indicates a rather high Jahn-Teller energy of the system. The distorted structure of K_2CuF_4 has also been observed by Tanaka *et al.* [22] as quoted by Hirakawa and Ikeda [23]. Further X-ray experiments are underway to check possible correlations between the planes.

It has to be noticed that the observed X-ray diffraction pattern does not allow to determine the actual lattice distortion. This could also be due, for example, to alternative small rotations of the fluorine octahedra around the c-axis. However, it seems, that only the cooperative Jahn-Teller distortion in the c-plane can give rise to ferromagnetic coupling between the Cu^{2+} ions. The following discussion will be based on the structure model shown in figure 8.

4.2 ANALYSIS OF THE ABSORPTION SPECTRA. — The absorption spectrum of K_2CuF_4 shows some features which seem to be unique for a copper salt. The rather well resolved near infrared bands contain a rich vibrational structure. In this section we firstly analyze the contributions of electric and magnetic dipole transitions within the different absorption bands. In a second part we shall show that the results can be interpreted in the elongated octahedron model as discussed in 4.1. Eventually we shall point out that a consistent description of the dichroism is only possible, if a local D_{2h} point symmetry of the Cu^{2+} ions is assumed.

4.2.1 *Electric and magnetic dipole contributions to the absorption spectrum.* — According to figure 2 it seems to be obvious that the bands B_3 (8 400 cm^{-1}) and B_1 (12 200 cm^{-1}) correspond to electric dipole transitions, since in both cases σ and α absorption are equal, but different from π absorption. This does not hold, however, for band B_2 (9 400 cm^{-1}) and its associated narrow lines. The α and σ absorptions of the broad band are only 75 % and 55 %, respectively, of the π absorption. This seems to indicate that both, electric and magnetic dipole mechanisms contribute to this band.

These two types of transitions are more clearly distinguished in the narrow lines at 8 766 cm^{-1} and 8 979 cm^{-1}. In the first case π and α absorption strengths are equal, whereas the σ absorption vanishes (Fig. 3). The actual difference between the line heights in π and α is merely due to different spectrometer resolutions, which were limited to 10 and 5 cm^{-1}, respectively (see 3.1). On the other hand, the 8 979 cm^{-1} line strength comes out to be equal in σ and α, whereas the line is practically absent in π polarization. Hence we can conclude that the 8 766 cm^{-1} line corresponds to a magnetic dipole allowed zero-phonon transition. Its oscillator strength at $T \sim 0$ is $f_{0\text{-}0} = 1.9 \times 10^{-8}$. Typically it lies at the long wavelength edge of the associated broad band. The 8 979 cm^{-1} line, on the other hand, may be attributed to an odd-phonon assisted electric-dipole transition (*false origin line*). The energy of the phonon involved corresponds to the energy difference of both lines : 213 cm^{-1}.

Further evidence for the contribution of magnetic-dipole mechanisms involved in the near IR transitions is derived from the temperature behaviour of the overall oscillator strength $f(T)$. We find deviations from the simple law

$$f(T) = f(0) \coth \frac{\hbar\omega}{2 k_B T}, \qquad (3)$$

which would be expected for a purely phonon-assisted electric dipole mechanism (cf. insert of Fig. 1). If we assume a temperature independent magnetic dipole contribution f_1, we therefore rather expect

$$f(T) = f_0 \coth \frac{\hbar\omega}{2 k_B T} + f_1, \qquad (4)$$

where f_0 is the electric dipole contribution at $T = 0$. The function

$$\operatorname{arcoth} \frac{f(T) - f_1}{f(0) - f_1} = \frac{\hbar\omega}{2 k_B T} \qquad (5)$$

should give a straight line through the origin in a plot versus $1/T$. This is indeed achieved with $f_1 = 0.2\, f(0)$ as a best fit parameter, when using our $f(T)$ data (lower line in the insert of Fig. 1). This result indicates that 20 % of the overall oscillator strength at $T = 0$ is due to magnetic dipole transitions. The value $f_1 = 4 \times 10^{-6}$ is in agreement with the order of magnitude generally expected [24].

If we assume that, in a first approximation, only the band B_2 contains magnetic dipole contributions, we can estimate the Huang-Rhys factor of the magnetic dipole transitions involved in B_2. By use of the formula

$$f_{0\text{-}0}/f_1 = e^{-S}$$

we find $S = 5.4$.

According to eq. (5), the slope of the respective line in the insert of figure 1 yields the energy of the odd phonons coupled to the Cu^{2+} complexes. We find an energy of 175 cm^{-1}, which agrees reasonably with the energy of the phonon being responsible for the 8 979 cm^{-1} line (213 cm^{-1}). It has to be borne in mind that ω in eq. (15) only represents an average energy of all odd phonons at $k = 0$, whereas the one-phonon line corresponds to one well defined odd phonon.

4.2.2 *Interpretation of the spectra assuming local* D'_{4h} *symmetry.* — 4.2.2.1 Tetragonal crystal field and spin-orbit coupling. — In this section we shall discuss the energy positions of the bands A, B_1, B_2 and B_3. It is well known that the energy of a purely electronic final state is given by the position of the associated zero phonon line, and not by the absorption band maximum. The 8 766 cm^{-1} line may thus be considered as the purely electronic origin of the 9 400 cm^{-1} band (B_2). The positions of the non-resolved zero-phonon lines belonging to B_1 and B_3 may tentatively be found on the respective low energy band edges. In order to do so, we have decomposed one of the spectra in figure 2 into three single bands, where symmetric band shapes have been assumed for B_1 and B_3. The positions of the respective zero-phonon lines are indicated by arrows. The energy values are listed in the following table I :

TABLE I

	Absorption band maximum	Zero-phonon line energy
	—	—
B_1	12 200 cm^{-1}	(9 100 ± 200) cm^{-1}
B_2	9 400 cm^{-1}	8 766 cm^{-1}
B_3	8 400 cm^{-1}	(5 300 ± 200) cm^{-1}
A	970 cm^{-1}	(900 cm^{-1})

The Cu^{2+} ion has the electronic configuration $3d^9$. A cubic crystal field splits the ^2D state of the free ion into a ground state doublet ^2E_g and an excited state triplet $^2T_{2g}$. The ground state degeneracy causes a tetragonal distortion of the nearest-neighbour fluorine octahedron by means of the Jahn-Teller effect. This distortion lifts the degeneracies of ^2E_g and $^2T_{2g}$ as is shown in figure 10.

The energy level scheme in this figure corresponds to elongated F^- octahedra. Before the introduction of the spin-orbit coupling, which will lift the degeneracy of $^2E_g(D_{4h})$, we can already predict that the different bands correspond to the following transitions :

$$A : {}^2B_{1g} \rightarrow {}^2A_{1g}$$
$$B_3 : {}^2B_{1g} \rightarrow {}^2B_{2g}$$
$$B_1 \text{ and } B_2 : {}^2B_{1g} \rightarrow {}^2E_g .$$

Let us consider now the effect of the spin-orbit coupling. It will be necessary to estimate at first the value of the spin-orbit coupling constant. This is possible by an evaluation of the g-factors $g_\parallel$ and $g_\perp$ as obtained by Yamada [5]. These values have been measured with respect to the crystal axes and not with respect to the relevant axes of the local crystal field. Let us define $g'_\parallel$ and $g'_\perp$ as the g-factors relative to the axes of the local octahedra. It is easily verified that :

$$g_\parallel = g'_\perp = 2.08 \tag{6}$$
$$g_\perp = \tfrac{1}{2}(g'_\parallel + g'_\perp) = 2.30 , \tag{7}$$

and hence $g'_\parallel = 2.52$ and $g'_\perp = 2.08$. Abragam and Bleaney [25] have calculated $g'_\parallel$ and $g'_\perp$ for the Cu^{2+} ion in an elongated ligand octrahedron :

$$g'_\parallel = 2 - \frac{8\lambda}{\Delta_0} \quad \text{and} \quad g'_\perp = 2 - \frac{2\lambda}{\Delta_1}, \tag{8}$$

where

$$\Delta_1 = E(^2E_g) - E(^2B_{1g}) \sim 9\,000 \text{ cm}^{-1} ,$$

and

$$\Delta_0 = E(^2B_{2g}) - E(^2B_{1g}) \sim 5\,300 \text{ cm}^{-1}$$

(see Fig. 10).

An evaluation of the eq. (6), (7) and (8) yields $\lambda = -360$ cm^{-1} and $\lambda = -345$ cm^{-1}. We thus conclude that λ must have a value of about -350 cm^{-1}, which is considerable reduced as compared with the free ion value (-830 cm^{-1} [26]). This reduction has to be attributed to covalency effects between the Cu^{2+} ion and the $2p_\sigma$ orbitals of the F^- ligands

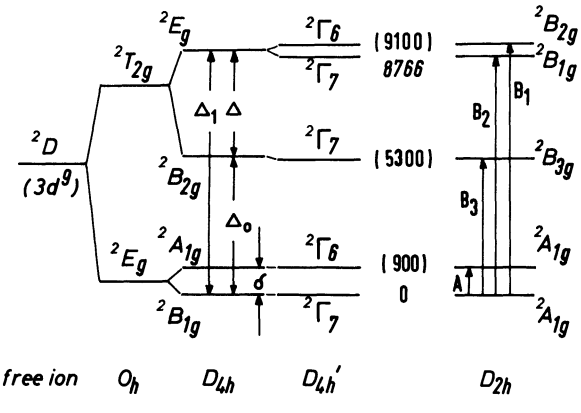

FIG. 10. — Energy level diagram of Cu^{2+} in K_2CuF_4, showing splitting due to crystal field (O_h, D_{4h}) and spin-orbit coupling (D'_{4h}). Excited state energies are given in cm^{-1}. In the righthand level scheme, referring to local D_{2h} symmetry, the optical transitions (arrows) are labeled with the respective absorption band notations.

[27], [23]. In the context of our discussion we restrict ourselves to notice that λ is very much smaller than the separation Δ of the $^2T_{2g}(O_h)$ sublevels, which arises from the tetragonal distortion.

Applying now the spin-orbit interaction to the Cu^{2+} ion in D_{4h}, we expect the following energies with respect to the $^2T_{2g}(O_h)$ level under the assumption $|\lambda/\Delta| \ll 1$ [25] :

$$E(^2B_{2g}) = -2\Delta/3 \rightarrow {}^2\Gamma_7(D'_{4h})$$
$$E'(^2E_g) = \Delta/3 + \lambda/2 \rightarrow {}^2\Gamma_7(D'_{4h})$$
$$E''(^2E_g) = \Delta/3 - \lambda/2 \rightarrow {}^2\Gamma_6(D'_{4h}) .$$

The sublevels are now characterized by their irreducible representations $^2\Gamma_6$ and $^2\Gamma_7$, respectively, in the double group $D'_{4h} = D_{4h} \times D_{1/2}$. The energy difference between E' and E'' comes out to be $\lambda \sim 350$ cm^{-1} in agreement with the estimated energy difference of the purely electronic origins of the bands B_1 and B_2 (see Table I). The energy separation $\Delta_1 - \Delta_0 = \Delta \sim 3\,700$ cm^{-1}, on the other hand, allows a determination of the parameters B_2^0 and B_4^0, which characterize the tetragonal component of the crystal field. We use the relations [21]

$$\Delta = 9\,B_2^0 + 60\,B_4^0 \sim 3\,700 \text{ cm}^{-1}$$
and (9)
$$\delta = 12\,B_2^0 - 60\,B_4^0 \sim 900 \text{ cm}^{-1} ,$$

where $\delta = E(^2A_{1g}) - E(^2B_{1g})$ is the energy splitting of $^2E_g(O_h)$ ground state level in D_{4h} (see Fig. 11). These equations yield $B_2^0 \backsim 220$ cm^{-1} and $B_4^0 \sim 30$ cm^{-1}. The value of B_2^0 thus obtained from the absorption spectrum is somewhat greater than the value $B_2^0 = 150$ cm^{-1}, which has been calculated by Le Dang Khoi [28] in a point ion approximation over a sphere of the radius 20 a (a = mean lattice constant of K_2CuF_4). The agreement is satisfying in view of the fact that a point ion model neglects covalency effects, which are rather important in K_2CuF_4.

Before we discuss the selection rules which determine the dichroism of the near IR absorption, we can note that the crystal field model using a local D'_{4h} symmetry yields quite reasonable energy values for the band positions. However, it does not allow one to unterstand why the B_1 level is more strongly coupled to the lattice than the B_2 level. There are two other effects, which might influence the behaviour of the $^2E_g(D_{4h})$ level. One is the Jahn-Teller effect, which could be effective, since the spin-orbit coupling energy is rather low [29]. On the other hand, it has to be taken into account that the local symmetry of the Cu^{2+} ion is lower than D_{4h} (D_{2h} in the paramagnetic state). The importance of the orthorhombic contribution to the crystal field is difficult to predict *a priori*. For the Jahn-Teller effect, a coupling of the $^2E_g(D_{4h})$ state with lattice modes of B_{1g} or B_{2g} symmetry in the x'y'-plane of the elongated F^- octahedron (see Fig. 8) can take place [29]. If the Jahn-Teller coupling to one mode is stronger than to the other, an absorption band presenting two peaks can be expected. In the case of local D_{2h} symmetry the orbital degeneracy of $^2E_g(D_{4h})$ will be lifted. Each of the resulting substates may be coupled to different lattice modes with different strengths, thus yielding different Huang-Rhys factors for both states. Even if the purely electronic origins of these states are nearly degenerate, two totally different broad sidebands can arise.

4.2.2.2 Selection rules in D'_{4h} symmetry. — We define π'_0 and α'_0 as electric-dipole absorption coefficients, where the electric vector of the absorbed photon lies parallel and perpendicularly, respectively, to the c' axis of the elongated ligand octahedron (see Fig. 8). On the other hand, π'_1 and α'_1, denote the magnetic-dipole absorption coefficients for the magnetic vector of the photon being parallel to c' and one of the a' axes respectively. In the system of the global crystal axes we can decompose the absorption coefficients in the following way :

$$\pi = 2\,\alpha'_0 + \pi'_1 + \alpha'_1 \qquad (\mathbf{E} /\!/ \mathbf{c} \text{ and } \mathbf{H} /\!/ \mathbf{a})$$
$$\sigma = \alpha'_0 + \pi'_0 + 2\,\alpha'_1 \qquad (\mathbf{E} /\!/ \mathbf{a} \text{ and } \mathbf{H} /\!/ \mathbf{c}) \quad (11)$$
$$\alpha = \alpha'_0 + \pi'_0 + \alpha'_1 + \pi'_1 \qquad (\mathbf{E} /\!/ \mathbf{a} \text{ and } \mathbf{H} /\!/ \mathbf{a}) .$$

In the system of the local octahedron **H** transforms like Γ_2^+ and Γ_5^+, if **H** is parallel or perpendicular to **c**', respectively. It is easily shown that magnetic dipole transitions $^2\Gamma_7 \rightarrow {}^2\Gamma_7$ and $^2\Gamma_7 \rightarrow {}^2\Gamma_6$ are allowed in either case. This result is in contradiction with our observations on the 8 766 cm^{-1} line, which only appears in π and α polarization.

The selection rules for phonon assisted electric dipole transitions are also readily obtained. It has to be taken into account that the odd parity phonons in D'_{4h} transform like Γ_2^-, Γ_4^- and Γ_5^-, and that the electric light vector transforms like Γ_2^- or Γ_5^-, if **E** // **c**' or **E** // **a**', respectively. It comes out that α' transitions are allowed for $^2\Gamma_7 \rightarrow {}^2\Gamma_7$ and $^2\Gamma_7 \rightarrow {}^2\Gamma_6$, whatever the symmetry of the odd phonon involved. In the π' polarization the transition $^2\Gamma_7 \rightarrow {}^2\Gamma_7$ is forbidden, if the excited state is only coupled to the Γ_4^- mode. The same selection rule applies to $^2\Gamma_7 \rightarrow {}^2\Gamma_6$, if coupling to all but the Γ_2^- mode is neglected. By use of the eq. (11) we find therefore that an electric dipole transition is never completely forbidden, in contradiction to the experimental result that the one-phonon line at 8 979 cm^{-1} is absent in π polarization.

4.2.3 *Interpretation of the spectra assuming local* D_{2h} *symmetry.* — Let us now consider the case that each elongated ligand octahedron undergoes a complementary deformation along the c-axis of the crystal, thus leading to a local D_{2h} symmetry. We define z' and x' to be the axes in the c-plane and y' to be parallel to c (see Fig. 8 : coordinate systems II*a* and II*b*). Furthermore we state that $y'z'$, $z'x'$ and $x'y'$ transform like the representations B_{1g}, B_{2g} and

B_{3g}, respectively, of the point group D_{2h}. If we call $\sigma_0^{x'}$, $\sigma_0^{y'}$ and $\sigma_0^{z'}$ the dipolar electric absorption coefficients for $\mathbf{E} /\!/ \mathbf{x}'$, $\mathbf{y}'$ and $\mathbf{z}'$, respectively, and if $\sigma_1^{x'}$, $\sigma_1^{y'}$ and $\sigma_1^{z'}$ are the dipolar magnetic absorption coefficients for $\mathbf{H} /\!/ \mathbf{x}'$, $\mathbf{y}'$ and $\mathbf{z}'$, we obtain :

$$\begin{aligned} \pi &= 2\,\sigma_0^{y'} + \sigma_1^{x'} + \sigma_1^{z'} \\ \sigma &= \sigma_0^{x'} + \sigma_0^{z'} + 2\,\sigma_1^{y'} \\ \alpha &= \sigma_0^{x'} + \sigma_0^{z'} + \sigma_1^{x'} + \sigma_1^{y'} . \end{aligned} \qquad (12)$$

Now the selection rules for magnetic dipole transitions from the ground state $^2A_{1g}(D_{2h})$ to the excited states $^2B_{1g}$, $^2B_{2g}$ and $^2B_{3g}$ are easily obtained by taking into account that $\mathbf{H} /\!/ \mathbf{x}'$, $\mathbf{y}'$, $\mathbf{z}'$ transforms like B_{1g}, B_{2g} and B_{3g}, respectively. The results are compiled in the following table II :

TABLE II

Magnetic dipole transitions of Cu^{2+} *in* K_2CuF_4 *assuming local* D_{2h} *symmetry*

Transition	π	σ
$^2A_{1g} \rightarrow {}^2B_{1g}$	allowed	forbidden
$^2A_{1g} \rightarrow {}^2B_{2g}$	forbidden	allowed
$^2A_{1g} \rightarrow {}^2B_{3g}$	allowed	forbidden

According to this table we deduce that the zero-phonon line at 8 766 cm^{-1} might be due to the transitions into $^2B_{1g}$ or $^2B_{3g}$. A straightforward calculation of the selection rules for electric dipole transitions, which are assisted by odd phonons transforming like B_{1u}, B_{2u} and B_{3u}, yields the following table III (+ = allowed, − = forbidden) :

TABLE III

Phonon assisted electric dipole transitions of Cu^{2+} *in* K_2CuF_4 *assuming local* D_{2h} *symmetry*

	B_{1u} Mode		B_{2u} Mode		B_{3u} Mode	
Transition	α	π	α	π	α	π
$^2A_{1g} \rightarrow {}^2B_{1g}$	−	−	+	−	−	+
$^2A_{1g} \rightarrow {}^2B_{2g}$	+	−	−	−	+	−
$^2A_{1g} \rightarrow {}^2B_{3g}$	−	+	+	−	−	−

According to this table it can be seen that strict selection rules for electric dipole one-phonon lines may exist. From the discussion concerning the 8 766 cm^{-1} line, we know that the 8 979 cm^{-1} line must correspond to either $^2B_{1g}$ or $^2B_{3g}$. Non-vanishing α absorption can only occur, if these states interact with a B_{2u} phonon, which transforms like y'.

On the other hand we know from simple symmetry considerations that $^2B_{3g}(D_{2h})$ corresponds to $^2B_{2g}(D_{4h})$ and to the band B_3. Hence the sharp lines at 8 766 cm^{-1} and 8 979 cm^{-1} must correspond to transitions into the $^2B_{1g}(D_{2h})$ level, which is essentially coupled to a B_{2u} phonon.

More difficult is the explanation of the broad band dichroism. In these transitions a great number of even phonons of different symmetries may be involved. They can cause a complete loss of the symmetry character of the odd phonon, which makes the transition allowed. However, if a predominant interaction with an odd phonon B_{2u} and the breathing mode A_{1g} is assumed, it is readily seen that the band B_3 must be stronger in σ than in π absorption. This could explain the large dichroism observed in B_3. The B_1 band, corresponding to $^2A_{1g} \rightarrow {}^2B_{2g}$ should not show a pronounced dichroism, since the B_{2u} mode does not lead to an allowed transition. If, however, the B_{1u} and B_{3u} modes interact with $^2B_{2g}$, the α absorption should be stronger than π in agreement with the experimental result.

In conclusion, it seems to be evident that the optical absorption spectra can only be explained with a structure model which includes an elongation of one of the local axes within the c-plane (Fig. 8) and a complementary deformation in c direction thus yielding local D_{2h} symmetry. It has to be noted, however, that a dynamical Jahn-Teller effect of the $^2E_g(D_{4h})$ state could probably result in a similar deformation [29].

It is interesting to remark that the lines between the 8 766 cm^{-1} and 8 979 cm^{-1} lines in the B_2 band exhibit practically the same dichroic behaviour as the zero-phonon line. Obviously these lines (8 833 and 8 884 cm^{-1}) correspond to even phonon sidebands of the magnetic dipolar line (Fig. 3). We have tried to measure the frequencies of these modes in a Raman scattering experiment ([3]), but no signal has been obtained at 77 K and 300 K for the different possible geometries.

4.3 MAGNETIZATION CURVES. — 4.3.1 *Out-of-plane anisotropy.* — In this section we shall discuss the magnetization curves, which have been obtained from MCD and Faraday rotation experiments (cf. 3.2.1 and 3.3 ; Fig. 4). They will be used to calculate the out-of-plane anisotropy field H_A of K_2CuF_4 at 4.2 K. The density of the anisotropy energy is given by [5]

$$E = K_1 \sin^2 \varphi + K_2 \sin^4 \varphi + K_3 \sin^2 \psi \cos^2 \psi \qquad (13)$$

where $K_{1,2,3}$ are the anisotropy constants, and $\varphi(\psi)$ is the angle between the magnetization vector and the c-axis (one of the a-axes) of the crystal.

The torque measurements of Yamada [5] and the MCD curves for $\mathbf{H} /\!/ \mathbf{a}$ (see 3.2.2) have shown that

([3]) This experiment has been performed on a double-grating Raman spectrometer Coderg using several argon laser lines. We like to thank P. Swartz for his help and the loan of his experimental equipment.

$K_3 \ll K_1$. Dropping the third term in (13) we therefore obtain

$$E(\varphi = 0) - E(\varphi = \pi/2) = \\ = -(K_1 + K_2) = \int_0^{M_s} H_i \, dM \quad (14)$$

for the magnetization energy in an axial field.

On the other hand, the anisotropy field H_A, lying in the c-plane, is defined via the torque density

$$L = | \mathbf{M}_s \times \mathbf{H}_A | = M_s H_A \cos \varphi = -\partial E/\partial \varphi \, . \quad (15)$$

In the limit $\varphi \to \pi/2$ one obtains from (13) and (15)

$$H_A = -2(K_1 + 2K_2)/M_s \, . \quad (16)$$

Since $K_2 \ll K_1$ [5], we can combine (14) and (16) to the final expression

$$H_A = 2 \int_0^{M_s} H_i \, dM/M_s \, . \quad (17)$$

Evaluating (17) by use of the dashed curve in figure 4, we find $H_A = 2\,400$ Oe. This should be compared with Yamada's value $H_A = 2\,800$ Oe.

The difference of both values cannot be due to our neglect of the in-plane anisotropy, which was estimated to be less than 50 Oe. We rather argue that the difference is due to different sample qualities used in both experiments. It is well-known that the anisotropy constants have to be determined on very pure single crystals with negligible hysteresis, in order to avoid supplementary energy barriers for the domain wall movement. In our crystal hysteresis was completely absent, whereas Yamada [5] reported some remanent magnetization of his samples. Since the detection limits of M were about equal in both experiments, we can conclude that our sample contained less lattice defects, thus yielding the lower H_A value. Unfortunately, Yamada's $M(H)$ curve has not been corrected for the demagnetization field. This rules out a direct comparison with our $M(H)$ curves.

4.3.2 *In-plane anisotropy.* — The magnetic field dependence of the linear birefringence in the ac-plane for $\mathbf{H} \,/\!/\, \mathbf{a}'$ (cf. 3.4 and Fig. 7) allows an estimation of the in-plane anisotropy with the following assumptions :

i) the change of the birefringence $| \Delta n(H) - \Delta n(0) |$ as a function of the applied field H is proportional to the field induced magnetostriction $\delta l/l$ in field direction,

ii) the magnetostriction can be calculated within a purely statistical model for the domain distribution, as proposed by Heisenberg [30].

The first assumption seems to be justified by the success of the compressible lattice model to explain the LMB of a magnetic crystal [11]. The second assumption is certainly a simplification, which, however, describes the magnetostriction of a soft ferromagnet rather well [30]. Since this condition is met in our samples (cf. 4.3.1), we have applied the theory of Heisenberg to K_2CuF_4, which has two easy directions of the magnetization within the c-plane. The calculations are similar to those applied to Fe [30], which has three easy directions parallel to $\langle 100 \rangle$. If n_+, n_-, $n_\perp$ are the numbers of domains with their magnetization parallel, antiparallel and perpendicular, respectively, to the field direction, we find :

$$n_+ = n(1 + \delta)^2/4 \, , \\ n_- = n(1 - \delta)^2/4 \, ,$$

and

$$n_\perp = n(1 - \delta^2)/2 \, ,$$

where $n_+ + n_- + n_\perp = n$ is the total number of domains, and $\delta = M/M_s$ is the relative magnetization of the sample. These numbers enter into the general formula describing the magnetostriction [30], which in our case comes out to be

$$\delta l/l = \lambda_0 \, \delta^2 \quad (18)$$

for the field induced striction in $\mathbf{a}'$ direction. λ_0 is the respective longitudinal magnetostrictive constant.

Eq. (18) combined with the assumption (i) leads to the relation

$$| \Delta n(H) - \Delta n(0) | \propto (M/M_s)^2 \, .$$

The solid line in figure 7 may therefore be interpreted as the square of the relative magnetization $(M/M_s)^2$ versus H. This is easily converted into M/M_s versus H (dot-dashed line in figure 7; righthand ordinate scale).

In order to obtain M/M_s as a function of the internal field H_i, we apply the same correction for the demagnetization field as described in 3.2.1. The resulting curve, M/M_s versus H_i, which now replaces H on the abscissa scale, is presented as a dashed line in figure 7. This curve begins nearly vertically at $H_i \sim 0$, and reaches a value of $M/M_s = 0.7$ at $H_i \sim 50$ Oe. This is about 20 times smaller than the respective H_i value for magnetization in c direction (see Fig. 4). This clearly demonstrates that the directions of the easy axes lie in the c-plane in agreement with the results of Yamada [5] and our MCD data (3.2.2). Saturation, however, needs a field of $H_i \sim 300$ Oe. This seems to indicate that a certain amount of the domain walls cannot move freely because of lattice defects, which have been introduced by the sample preparation (sample II had necessarily to be sawn and polished, since it does not contain cleavage planes).

5. **Conclusion.** — We have tried to describe the d-d transitions of Cu^{2+} in K_2CuF_4 within the crystal

field approximation. The following data have been taken into account :

i) the peak energies of four absorption bands in the near infrared and the positions of two sharp lines, corresponding to zero- and one-phonon transitions, respectively,

ii) the anisotropy of the **g**-tensor,

iii) the linear dichroism of the broad bands and of the lines.

It turns out to be necessary to assume that the Cu^{2+} ions are surrounded by elongated ligand octahedra, the long axes of which being alternatively parallel to the x and y directions within the c-planes of the crystal. X-ray structure investigations seem to confirm this assumption. A complete energy level scheme can be established by taking into account local D_{4h} symmetry and the spin-orbit coupling ($\lambda = -350$ cm^{-1}). In order to explain the linear dichroism, an additional orthorhombic distortion of the ligand octahedra must be assumed. The absorption is mainly due to electric dipolar phonon assisted transitions, but a magnetic dipolar contribution to the broad band absorption becomes evident from its dichroic behaviour and from the temperature dependence of its oscillator strength.

Several optical properties of K_2CuF_4 prove to be related to ferromagnetic order below $T_c = 6.25$ K. The MCD and the Faraday rotation are proportional to the macroscopic magnetization. The $M(H)$ curves thus obtained allow a determination of the anisotropy field. The magnetic field dependence of the linear birefringence within the c-plane proves to be proportional to the square of the in-plane magnetization. The circular dichroism, measured on single domains, seems to be promising as a means of measuring the temperature dependence of the spontaneous magnetization.

Acknowledgments. — We like to thank F. Denoyer, Le Dang Khoi, F. Moussa and R. H. Silsbee for valuable discussions on the magnetic, optical and structural properties of K_2CuF_4. The performance of X-ray diffraction studies by F. Denoyer and the help with Raman experiments by P. Swartz are greatly appreciated.

References

[1] Recent review articles, containing many references are given by :
De Jongh, L. J., Miedema, A. R., *Adv. Phys.* **23** (1974) 1 and Hone, D. W., Richards, P. M., *Annu. Rev. Mater. Sci.* **4** (1974) 337.
[2] Mermin, N. D., Wagner, H., *Phys. Rev. Lett.* **17** (1966) 1133.
[3] Stanley, H. E., Kaplan, T. A., *Phys. Rev. Lett.* **17** (1966) 913.
[4] Yamada, I., *J. Phys. Soc. Japan* **28** (1970) 1585.
[5] Yamada, I., *J. Phys. Soc. Japan* **33** (1972) 979.
[6] Gupta, L. C., Vijayaraghavan, R., Damle, S. M., Rao U. R. K., Le Dangh Khoi, Veillet, P., *J. Magn. Reson.* **17** (1975) 41.
[7] Day, P., Gregson, A. K., Leech, D. H., *Phys. Rev. Lett.* **30** (1973) 19.
[8] Gregson, A. K., Day, P., Fair, M. J., private communication as quoted in ref. [9].
[9] Hutchings, M. T., Gregson, A. K., Day, P., Leech, D. H., *Solid State Commun.* **15** (1974) 313.
[10] Kleemann, W., Farge, Y., *J. Physique Lett.* **35** (1974) L-135.
[11] Jahn, I. R., Dachs, H., *Solid State Commun.* **9** (1971) 1617; Jahn, I. R., *Phys. Stat. Sol.* (b) **57** (1973) 681.
[12] Jahn, I. R., Bittermann, K., *Solid State Commun.* **13** (1973) 1897.
[13] Kleemann, W., Pommier, J., *Phys. Stat. Sol.* (b) **66** (1974) 747.
[14] Khomskii, D. I., Kugel, K. J., *Solid State Commun.* **13** (1973) 763.
[15] Régis, M., Farge, Y., *J. Physique* (to be published).
[16] Kubo, H., Shimohigashi, K., Yamada, I., *J. Phys. Soc. Japan* **34** (1973) 1687.
[17] Hirakawa, K., Ikeda, H., *J. Phys. Soc. Japan* **33** (1972) 1483; **35** (1973) 1328.
[18] Chen, E. Y., Dillon, Jr., J. F., Guggenheim, H. J., Proc. Conf. Magn., Boston (1973).
[19] Suits, J. C., Argyle, B. E., Freiser, M. J., *J. Appl. Phys.* **37** (1966) 1391.
[20] Knox, K., *J. Chem. Phys.* **30** (1959) 991.
[21] Drumheller, J. E., Dickey, D. H., Rehlis, R. P., Zaspel, C. E., Glass, S. J., *Phys. Rev. B* **5** (1972) 4631.
[22] Tanaka, K., Akimitsu, J., Saito, N., as quoted in reference [23].
[23] Hirakawa, K., Ikeda, H., *Phys. Rev. Lett.* **33** (1974) 374.
[24] Sugano, S., Tanabe, Y., Kamimura, H., *Multiplets of Transition Metal Ions in Crystals* (Acad. Press, New York, London) 1970.
[25] Abragam, A., Bleaney, B., *Electron Paramagnetic Resonance of Transition Ions* (Clarendon Press, Oxford) 1970.
[26] Shenstone, A. G., Wilets, J., *Phys. Rev.* **83** (1951) 104.
[27] Hirakawa, K., Ikeda, H., *J. Phys. Soc. Japan* **35** (1973) 1608.
[28] Le Dang Khoi, private communication.
[29] Ballhausen, C. J., *Theor. Chim Acta* **3** (1965) 368.
[30] Heisenberg, W., *Z. Phys.* **69** (1931) 287.